Giant Vesicles Compressed by Actin Polymerization

by

Hyman A. Carrel

B.A. Physics
Cornell University, 2001

SUBMITTED TO THE DEPARTMENT OF PHYSICS IN PARTIAL FULFILLMENT OF THE REQUIREMENTS FOR THE DEGREE OF

MASTER OF SCIENCE
AT THE
MASSACHUSETTS INSTITUTE OF TECHNOLOGY

Author.....
Department of Physics
May 12, 2004

Certified by.....
Alexander van Oudenaarden
Assistant Professor of Physics
Thesis Supervisor

Certified by.....
Mehran Kardar
Professor of Physics
Thesis Reader

Grade.....

Accepted by.....
Thomas J. Greytak
Associate Department Head for Education

Giant Vesicles Compressed by Actin Polymerization

by

Hyman A. Carrel

Submitted to the Department of Physics
on May 12, 2004 in Partial Fulfillment of the
Requirements for the Degree of Master of Science

ABSTRACT

Actin polymerization plays a critical role in generating propulsive force to drive many types of cell motility. The discovery of actin based motility of the bacterial pathogen *Listeria monocytogenes* has lead to clearer understandings of the essential ingredients required for cell motility. The biophysical mechanisms by which these proteins generate forces is the subject of intense investigation. A novel system to study force generation by this polymerization engine is introduced by combining the well characterized mechanical properties of synthetic Giant Vesicles with the well understood biochemistry of actin polymerization. Giant Vesicles mimic the structural features of eukaryotic cell membranes. We find that Giant Vesicles coated with a protein that catalyzes actin polymerization form thick actin shells which produce a compressive force. The polymerization force directed at the membrane interface causes the membrane to rupture. In the resulting collapse we find that the shell thickens inward with a constant radial velocity and is characterized by radial lines of lipid and actin. We show that actin polymerization is the primary force driving the collapse.

Supervisor: Alexander van Oudenaarden
Title: Assistant Professor of Physics

Table of Contents

I. INTRODUCTION

EUKARYOTIC CELL MOTILITY

Movement is an essential characteristic of living organisms. Macroscopic movement has its origin at the cellular level. Fibroblasts are endothelial cells which can move synchronously to heal wounds. Keratocytes are a particularly mobile type of fibroblast. In blood vessels, neutrophils crawl to catch germs. Similarly, the amoeba Dictyostelium *discoideum* tracks and eats bacteria. Cell movement is very complex, involving signaling, transduction of chemical potential energy to directed forces, and the interplay of many physical and regulatory elements. The mechanical aspects of the movement of cells may be described by three distinct events: protrusion, translocation and detachment (Ref 21). Protrusion involves the extension of the membrane in specific directions through the formation of thin long projections called filopodia and of large flat sheet-like constructions called lamellipodia. Translocation involves the attachment of the lamellipodia to the substrate at locations in the cell membrane known as focal adhesion sites and the subsequent contraction of the cell by myosin motor proteins. Detachment involves further contraction of the rear of the cell to break the weakest cell-substrate bonds, thereby moving the mass of the cell forward. Protrusion involves actin, a 43 kDa protein which has two forms: G-actin is monomeric and F-actin is a helical polymer. Actin polymerization is thought to power the motility of eukaryotic cells by the growth of polymers against the cell membrane, through the addition of monomeric actin. During motility, actin has been visualized at very high densities as cross-linked filaments at the leading edge of the cell. Actin treadmills (Ref 41), meaning that actin filaments consist of rapidly polymerizing actin at one end and depolymerizing actin at the other end in a directed fashion. This process maintains a high actin monomer density, which in turn facilitates rapid polymerization, causing movement. Actin filaments do spontaneously grow from both ends although the barbed end grows much faster than the pointed end. The discovery of a bacteria which can control some of the hundreds of proteins responsible for animal cell movement has greatly aided the understanding of actin polymerization based motility.

LISTERIA MOTILITY AND ACTIN POLYMERIZATION

The bacterial pathogen *Listeria monocytogenes* has been studied extensively both to prevent its existence as a food born illness and to understand its striking manner of locomotion. Residing in food, *L. monocytogenes* allows itself to be phagocytosed by endothelial cells of the small intestine. The bacterium releases a pore forming toxin, listeriolysin O, which secures its release

from the endocytic vesicle into the host cells' cytoplasm. *L. monocytogenes* replicates itself before producing surface proteins that utilize the host cell's own motility machinery to propel the bacterium through the cytoplasm and into adjacent cells (Ref 5). Work on understanding *L. monocytogenes* (Ref 18) revealed that the only bacterial protein essential for motility in a host cell (or host cell extract), is the surface-bound virulence factor ActA which binds actin indirectly through Arp2/3 and VASP (Ref 39). Although hundreds of proteins are involved in regulating cell motility, the proteins essential for producing movement in L. *monocytogenes* have been isolated. To understand the system, we must understand its several parts. The actin related protein (Arp)2/3 complex is activated by ActA and aids polymerization via nucleating F-actin filaments to branch at 70º from existing filaments, cross-linking filaments and capping pointed ends (Ref 5). Vasodilator-stimulated phosphoprotein (VASP) is a focal adhesion protein which binds F-actin, profilin and ActA, and increases the branch spacing of filaments (Ref 33). Capping proteins block actin polymerization and depolymerization at the barbed ends. Gelsolin acts like a capping protein, but also has a role in severing actin filaments. α-actinin aids in crosslinking actin filaments. The protein actin depolymerizing factor (ADF, a.k.a. cofilin) has been shown to bind actin filaments, thereby increasing the rate of depolymerization from the pointed end (Ref 7, Ref 31). Since this is the rate limiting step in treadmilling, cofilin accelerates protrusion and *L. monocytogenes* propulsion. Profilin forms a complex with ATP-G-actin to increase polymerization exclusively at barbed ends. While ADF and profilin are not essential for motility, they do greatly enhance treadmilling (Ref 7). The rate of depolymerization is constant everywhere in a *L. monocytogenes*' comet tail (Ref 5).

As we approach a novel reduced system to study actin polymerization, it is useful first to understand several other intermediate model systems that measure the modality of force transduction. Study of *L. monocytogenes* actin motility has allowed motility to be introduced into several reduced systems.

MODEL SYSTEMS TO STUDY ACTIN POLYMERIZATION

Rigid model systems: Beads

The only bacterially produced protein that is essential for motility, ActA, has been transferred to several other systems in order to better understand the mechanisms and roles of the essential players in force generation. Polystyrene beads provide excellent substrates on which to observe actin polymerization. They provide a well characterized surface both physically and chemically, and they permit a varying of parameters both biochemical (e.g., ActA and Arp2/3 concentration) and physical (e.g., temperature, viscosity, or ActA distribution). In addition, beads have been

shown to undergo interesting dynamics such as hopping (Ref 3), steady-state gel thickness (Ref 30), and symmetry-breaking phenomena (Ref 38). Through understanding the usefulness of rigid substrate systems the great advantage of deformable substrate systems will be clear.

The protein ActA and a functionally homologous protein N-WASP (a variant of the Wiskott-Aldrich syndrome protein), which localizes to the membrane in eukaryotic cells, have been attached to polystyrene beads to produce motility similar to that of *L. monocytogenes*. In *Xenopus laevis* (African clawed frog) egg cytoplasmic extract, beads with diameters over 0.5 μm generated clouds of actin and remained stationary. However, smaller beads were seen to break symmetry after incubations of ~1 hour (Ref 6, Ref 38). Within three minutes of breaking symmetry, which is characterized by a wiggling of the bead within the actin cloud, the bead would choose a direction and move under actin polymerization at a blistering ~ 0.12 μm/s.

The motility of beads coated with the VCA domain of N-WASP was studied both in a reduced system of purified proteins and in a cell-free HeLa extract derived from a human HeLa S3 cell line by Bernheim-Grosswasser *et al.* (Ref 3). Both systems showed the same qualitative phenomenology: small beads (< 3 μm) showed smooth movement, while larger beads (3 μm) showed choppy movement, and still larger beads (≥ 4.5 μm) showed a periodic hopping movement on a time scale of ~10 minutes. Lower speeds, higher percentage moving and more symmetry-breaking was reported in purified protein mixtures. Symmetry-breaking was studied in this system, finding a that time of symmetry-breaking increases linearly with bead diameter (5 - 25 minutes for 1 - 9 μm beads).

Force Velocity Relation for *Listeria* and Beads

The polymerization of actin filaments uses chemical energy to perform physical work. In this way, ActA based actin polymerization is a type of motor. The mechanisms of this 'motor' are poorly understood, but two experiments have probed dependence of the propelled velocity on the opposing forces. McGrath *et al*. (Ref 25) considered the motion of *L. monocytogenes* in a viscous solution. Wiesner *et al*. (Ref 40) utilized beads in viscous solutions. Their results are not entirely consistent, but they do give insight into the force velocity relation.

McGrath *et al*. measured the response of *Listeria* motion to changes in viscosity (load) of diluted *Xenopus* egg extract. They found that for small loads (10-20 pN) there is a strong dependence on viscosity by the velocity (4.2-0.6 μm/min), but for loads up to (250 ± 120) pN the velocity changed slowly with load. An important result is that an increase in actin gel density by only 1.6 fold caused a 20 fold increase in force generated.

Wiesner *et al*. introduced N-WASP coated beads into a motility medium of purified proteins. The velocity of the beads was observed to be independent of bead size and the viscosity of the medium. Beads (diameters 0.2 μm - 3 μm) moved at a velocity of ~1 μm/min at a viscosity of 4 Pa-s (1 Pa-s = 10^3 centipoise). 2 μm diameter beads moved at ~1 μm/min in media of viscosity ranging from 10^{-3} Pa-s (water) to 3 Pa-s (measured) to 100-300 Pa-s (extrapolated). The bead velocity's observed independence of size and viscosity over five orders of magnitude implies that the propulsive force generated by the actin tail is large compared to the estimated 60 pN friction force for Stokes drag[1].

Additionally, Wiesner *et al*. sought to discover if Arp2/3 binds to filaments in the tail or only becomes part of the filament during branching at the bead surface. By adding fluorescently labeled Arp2/3 during motility, Wiesner *et al.* showed that Arp2/3 causes branching only at the bead surface and remains bound to the filament (showing up in the tail). Arp2/3 is an important motility constituent because branching increases the gel density and rigidity.

The importance of varying the viscosity of the medium in experiments with *L. monocytogenes* or with beads is that it allows the extraction of a force velocity curve. It is difficult to reconcile the two group's disparate results. Resolution would likely come from parallel viscosity measurements between purified components and diluted Xenopus extract. An interesting addendum is that the size independence of the velocity measured by Wiesner *et al.* conflicts with the inverse diameter dependence which Bernheim-Grosswasser *et al.* (Ref 3) measured, also in a mixture of purified proteins.

Actin forms an elastic gel

The physical properties of polymerized actin filaments pushing a bead or bacterium are an essential part of understanding force generation during cell motility. Gerbal *et al*. measured the physical properties of a comet tail removed from a motile *L. monocytogenes.* 2 μm polystyrene beads were fastened to the tail and multiple optical traps exerted forces on the beads to bend the tail. The tail was treated as a bent rod of an isotropic homogenous elastic material for calculation purposes. The bending of the tail matched this elastic model well and a Young's modulus was calculated to be 10^3-10^4 Pa (Ref 12).

Much work has been done on the elastic and viscoelastic properties of an actin gel (Ref 23, Ref 17). Although the comet tail has elastic properties that match those of an isotropic homogenous elastic material, more interesting phenomena result from actin density variations. McGrath *et al*. has shown that the actin gel becomes more dense when the polymerization is opposed (such as by pushing a greater load) (Ref 24). Gerbal *et al*. found a comet tail forming

Listeria mutant whose motion consists of nearly stationary behavior punctuated by periodic bursts of speed (up to 1 μm/s) (Ref 11). Periodic spots of dense actin in a comet tail combined with these great bursts of speed imply that these dense regions of actin are storing and releasing elastic energy.

A Flexible Model System: Vesicles

Large Vesicles (1 - 6 μm)

The deformation and density of a gel can yield information about the forces on a gel. Rigid structures such as a bacterium or a bead have been insufficient to visualize and to understand the forces that the gel itself exerts. This need for deformable substrates has been met by two groups who have used the ActA coated phospholipid vesicles to probe these forces. Actin polymerization has been shown to deform vesicles and form comet tails on these vesicles. These vesicles are originally quasi-spherical and are deformed into a teardrop shape and sometimes further elongated. Upadhyaya *et al*. (Ref 36) and Giardini *et al.* (Ref 13) used the deformation of vesicles to calculate a spatial force distribution on the surface of the vesicle. This showed that the actin gel is exerting a squeezing force on the sides of the vesicle and a retractile force on the back (point of the teardrop) of the vesicle. The presence of retractile forces implies that the vesicle is attached to the actin gel. Both groups found that the ActA distribution on the surface of a motile vesicle is polarized. Since phospholipid vesicles generally have high rates of lateral diffusion, the polarization of ActA shows that it does attach to the actin gel.

The motion observed in bovine brain extract consisted of an average velocity of (0.8 ± 0.2) μm/min made up of a periodically slow velocity and deformation followed by a rapid return to a quasi-spherical shape associated with a faster velocity. (Ref 36) Separately, the motion observed in *Xenopus* egg cytoplasmic extract consisted of an average velocity of (3.0 ± 2.4) μm/min made up of continuous changing deformation and speed (Ref 13).

INTRODUCTION TO OUR EXPERIMENTAL SYSTEM

Drawbacks to large vesicles

Large vesicles show motility originating from individual vesicles being pinched off from aggregates to develop comet tails. These aggregates introduce an inherent asymmetry in the system that prevents the study of symmetry-breaking during comet tail formation. Although the deformations of the vesicles can be analyzed to yield force estimates, the forces on the vesicles cannot be directly measured. Estimates of vesicle properties are based on unilamellar vesicles because multilamellar vesicles introduce further complications such as bilayer shifting and a

dynamic area expansion modulus under tension. Furthermore, large vesicles are sufficiently small to make it difficult to determine whether they are unilamellar.

Giant Vesicles offer increased control and precision

We need an improved system that has none of these drawbacks. Because each Giant Vesicle polymerizes actin independently, producing no inherent asymmetry, it allows us to view early stages of symmetry-breaking before comet tail formation. We can characterize the mechanical properties of Giant Vesicles and specifically measure the properties of each Giant Vesicle prior to use in an experiment. A pipette could be used to directly quantitate the forces of actin polymerization on a Giant Vesicle. Giant vesicles also offer a practical and mechanical advantage because methods exist to form Giant Unilamellar Vesicles (Ref 2).

Giant Vesicles studied with micropipettes

A dramatic advantage to working with Giant Unilamellar Vesicles lies in their use as finely calibrated transducers of force (Ref 10). The mechanical properties of Giant Vesicles have been well characterized. The bending modulus (k_c) and area expansion modulus (K_a) has been measured for Egg PC vesicles (used by Upadhyaya et al.) at 22ºC to be $k_c = (4 \pm 1.3) \times 10^{-5}$ nN-μm and $K_a = 190$ nN/μm, and for SOPC vesicles (experiments reported here) at 18°C $k_c = (9.0 \pm 0.6) \times 10^{-5}$ nN-μm and $K_a = 190$ nN/μm.

Giant Vesicles can contain actin

The previous systems have had the advantage of polymerizing actin directly at a surface. The vesicles' surface is similar to a cell membrane in that it is deformable. Although actin has not yet been polymerized directly at the surface of Giant Vesicles, actin has been polymerized within Giant Vesicles. Giant Vesicles have been loaded far above the critical concentration with actin monomers, and polymerization initiated by increasing the temperature or allowing an influx of ions. Miyata *et al*. (Ref 26) studied deformations due to actin polymerization within giant liposomes that occurred over time scales of 30-100 seconds. Liposomes were swelled at 0°C from a lipid film in a medium of G-Buffer[2], 100 mM Sucrose and 0.4 mg/mL BSA containing G-actin (100 μM or 200 μM). After swelling, 1 μL liposome solutions were mixed with 500 μL G-Buffer and 100 μM glucose solution. To this solution was added 500 μL G-Buffer with 60 mM KCl. KCl was introduced by electroporation to initiate polymerization within the liposomes. These solutions contain far lower ion concentrations than those used in ActA based motility

experiments, and so it remains a challenge to do ActA based motility experiments inside Giant Vesicles.

Actin within giant vesicles has been visualized in bundled filaments (Ref 14, Ref 26, Ref 21). Honda *et al*. (Ref 16) initiated actin polymerization by an increase of temperature while Sackmann *et al.* (Ref 22) increased the influx of Mg^{2+} ions through ionophores. Actin polymerization within giant vesicles has produced impressive results of protrusions and shells of actin filaments bonded to giant vesicles, producing viscoelastic membranes (Ref 15). However, in these previous experiments, polymerization of actin was not directed at the membrane since there was no protein that is functionally homologous to ActA. We use a new system to study actin polymerization that is directed at the surface of Giant Vesicles, the situation most likely to produce motility in cells.

USEFUL THEORETICAL MODELS AND TOOLS

Elastic continuum models for *Listeria* and vesicle propulsion

The primary models describing force generation at the interface of an actin gel are elastic continuum models by Noireaux *et al*. (Ref 30), by Gerbal *et al*. (Ref 11), and by Upadhyaya *et al*. (Ref 36) We can also consider a discrete molecular model by Mogilner and Oster (Ref 29). The model by Noireaux *et al*. considers ActA coated polystyrene microspheres, which are observed to grow actin gels up to a steady state thickness. The actin that polymerizes at the surface of a bead with a given density of ActA is considered to be a thin unstressed elastic shell. As subsequent shells polymerize, the previous shells are displaced outwards, becoming stretched. These stretched shells exert a compressive force. The thickness is explained by balancing the gain in chemical potential energy from adding a monomer to a filament with the cost in elastic energy (work) due to intercalating a monomer between the surface and the gel. If we consider a bead of radius r_i, the gain in chemical potential energy by inserting a shell of thickness e is proportional to the surface area of the shell, the surface density of ActA and the gain in chemical energy by adding a monomer. The work necessary to add a monomer to a filament is equal to the size of the monomer (a = 2.7 nm) times the product of the normal stress in the gel at the point of addition ($\sigma_\perp$, a pressure) and the area per filament ($d^2 = (25\ \text{nm})^2$). The elastic energy cost to insert the same shell is proportional to this work times the surface area of the shell. On a solid sphere the divergence of the stress in mechanical equilibrium must be zero. We find the normal stress on a spherical surface at a gel interface (r_i) is given by solving the equilibrium equation for the stress due to a gel of a thickness e, giving

$$\sigma_\perp(t) = 2Y\left[\frac{r_e^2(t)}{r_i^2}\left(\frac{r_e(t)}{r_i} - \frac{1}{2}\right) + \frac{1}{6}\right] \qquad (1)$$

where Y is the Young's modulus of the gel and r_e is the thickness of the gel.

The stacked rubber band model by Gerbal *et al*. (Ref 11) extends Noireaux *et al*.'s model of elastic shells to explain why *Listeria* breaks the symmetry inherent in an actin cloud to form a stable comet tail that produces powerful and directed motion. A build-up of elastic deformations within an actin gel that surrounds only half of a bacterium (treated as a rigid cylinder) can relax only by being pushed up and back at a constant volume into the bacterial comet tail.

Both of these models are limited by considering only rigid substrates for actin polymerization. Upadhyaya *et al*. describes the motion of comet tail forming stepping vesicles by

considering forces built up primarily within the deformable vesicle. Energy is stored in the stretching and the bending of the phospholipid membrane. However, it is the polymerization of actin and stress due to the actin gel that produces this energy. The model utilizes a release of energy due to a fracture of the actin to lipid bonds to produce the stepping, which corresponds to much of the vesicle's movement. This fracture of the bonds between actin filaments has also been used to explain the saltatory motion observed in beads (Ref 3) and *Listeria* (Ref 11).

Specifically, Upadhyaya *et al.* considers the volume change of a unilamellar vesicle of constant surface area which is squeezed on one hemisphere by an actin gel. The bare side of the vesicle forms a spherical cap, characterized by principal curvatures κ_1 and κ_2. The actin pressure is balanced by the induced osmotic pressure. The membrane tension is isotropic so the stress due to stretching in the spherical cap is equal to the osmotic pressure, $\Pi = -\tau(\kappa_1 + \kappa_2)$. At other points on the vesicle, actin polymerization balances the total stress, given by the sum of the osmotic pressure plus the local tensile stress. $\sum_x = \Pi + \sigma_x = -\tau((\kappa_1 + \kappa_2) - \kappa_x)$ which is proportional to the difference of the curvature in the cap from that at any other point in the vesicle (Ref 36). The osmotic pressure on the vesicle is

$$\Pi = RT(\frac{n}{v} - C_o) \qquad (2)$$

The area stretching of a unilamellar vesicle has an entropic stretching logarithmic term and a linear stretching term:

$$\alpha = \frac{k_B T}{8\pi k_c} \ln\left(1 + \frac{\tau \lambda_{\min}^2}{\pi^2 k_c}\right) + \frac{\tau}{K_a} \qquad (3)$$

where $\alpha = (A-A_o)/A_o$, k_B is Boltzmann's constant, T is temperature, k_c is the elastic bending modulus of the lipid bilayer, λ_{min} is the shortest wavelength of membrane undulation (Ref 10).

How does actin polymerization, due to the microscopic event of a single actin monomer elongating an actin filament on the molecular level, generate force on a intermediate level? The elastic brownian ratchet model (Ref 28) sought to explain this by considering filament tips thermally fluctuating next to a load (e.g., cell membrane, bacterium). When filament tips are near the load, they do not have the space to insert an additional monomer, but filament tips which fluctuate away from the load acquire the space needed to polymerize an additional monomer. These longer tips are compressed, generating the force to propel the load, and thereby rectifying thermal energy. However, this model failed to describe a gel-substrate attachment observed in beads, bacteria and vesicles (Ref 24, Ref 20, Ref 36). A revised 'tethered ratchet' model assumes that filaments attach transiently to the surface: surface proteins on the load initiate new filaments

that are held in tension between the cross-linked filaments and the load. As the filaments are released, they grow as described in the brownian ratchet model until they are capped (Ref 29).

These models utilize a polymerization velocity of actin filaments (v_p) that depends on the relaxed polymerization velocity of actin filaments (v_{po} = 2 μm/min) and the stress in the actin gel:

$$v_p = v_{po} \exp\left(-\frac{W}{k_B T} \right) \tag{4}$$

where W is the work to intercalate a monomer. This work is the given by

$$W = \sigma_{\perp} a d^2 \tag{5}$$

where $\sigma_{\perp}$ is the stress normal to the surface. The exponential dependence on stress is attributed to the difficulty of intercalate monomers at an interface that involves large normal stresses.

II. RESULTS

MATERIALS AND METHODS

Giant Vesicle Electroformation

Our system consists of giant phospholipid vesicles containing 90% 1-Stearoyl-2-Oleoyl-sn-Glycero-3-Phosphocholine (SOPC) and 10% 1,2-Dioleoyl-sn-Glycero-3-[N-(5-amino-1-carboxypentyl)iminodiacetic acid)succinyl] (DOGS-NTA) . To this mixture we add a fraction of fluorescent lipids, 1% w/v 1,2-Dioleoyl-sn-Glycero-3-Phosphoethanolamine-N-(7-nitro-2-1,3-benzoxadiazol-4-yl) (18:1 NBD PE) (all from Avanti Polar Lipids) or 0.5% Oregon Green® 488 1,2-dihexadecanoyl-*sn*-glycero-3-phosphoethanolamine (Oregon Green® 488 DHPE) (Molecular Probes). Giant Vesicles are formed by the electroformation method of Angelova (Ref 1, 2), using indium tin oxide (ITO) coated glass slides[3] in 215 mOsm sucrose solution. The slides are stored desiccated to minimize water condensation on the slide surface. The resistance of each slide is measured using a multimeter (73 III, Fluke) and is (50 ± 20) Ω. Immediately before use, the conducting face is roughened by vertical strokes with a razor blade. The lipids are dissolved to 1 mg/mL in a 2:1 mixture of chloroform and methanol in a 1.5 mL glass centrifuge tube. The total volume is ~330 μL (much larger than a typical sample volume) to minimize concentration variations due to evaporation between initiation of mixing and coating of slides (~20 minutes). The lipids are added and mixed gently with glass gas-tight syringes (Hamilton Co.). The syringes are washed with chloroform before adding new lipids. A nickel-sized region of each ITO coated slide is coated uniformly with 5-6 μL lipid mixture. The slides are dried under compressed air for 2 minutes and placed in a desiccator under vacuum for 1 hour. A roll of lab tape (Laboratory Labeling Tape, VWR) is made more sticky by heating with a heatgun (Master Appliance Corp, Racine, WI). A 2 inch length of copper wire (18 AWG) is roughened with a file to improve conduction and taped with the heated lab tape to the ITO slides. A polypropylene ring covered with vacuum grease (Dow Corning) is used as a spacer between the slides. The slides are filled with excess sucrose solution (to prevent air bubbles) and the chambers are held closed with small binder clips (Acco).

The chamber is immediately attached by alligator clips to a function generator (Jupiter 2010 2 MHz, Tenma®) and the frequencies and voltages are varied as given in Table 1.

Table 1. Settings for Electroformation

Frequency (Hz)	Voltage (V)	Time (min)
10	3.0	50
3.1	2.75	40
1.8	2.5	20
1.1	2.5	10
Off	0	10

The chambers are opened and the solution is pipetted into a glass microcentrifuge tube. All GUV solutions are stored at room temperature. Solutions containing fluorescent lipids are stored in darkness for up to a week.

Attaching ActA to Giant Vesicles

The nickel chelating lipids are used to bind to the histidine tag on the ActA molecules. The ActA has been purified from a strain of *Listeria monocytogenes* (a kind gift of D. Portnoy). The ActA purification process is described by Cameron *et al*. (Ref 6) and Upadhyaya *et al*. (Ref 36)

After relaxing overnight (Ref 9), the vesicles are incubated with an equal volume of ActA for ~ ½ hr at a saturating ActA concentration.

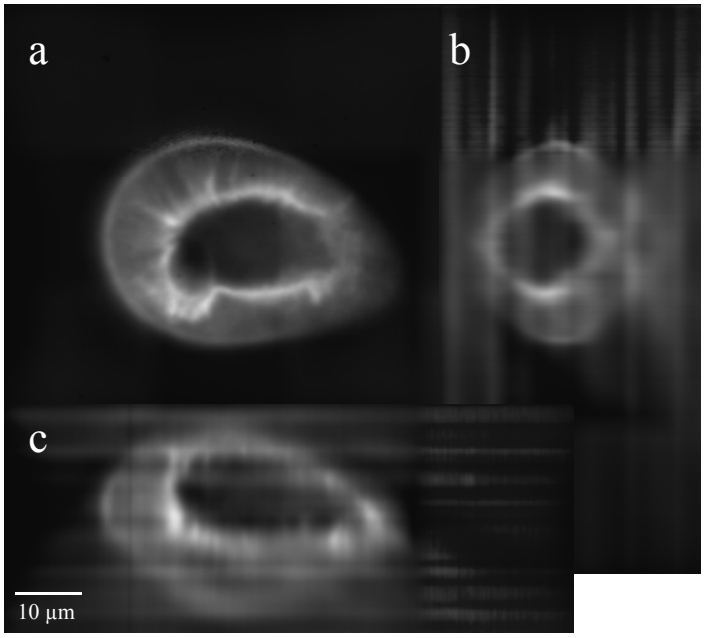

Figure 1. Structure of a crushed Giant Vesicle. The actin shell that has crushed a Giant Vesicle is shown by rhodamine-labeled actin in slices from a 3D deconvolved image in (a) XY (b) ZY and (c) XZ planes.

Motility Assay

All dynamics experiments were performed in 25 μL bovine brain extract, 25 μL assay buffer (20 mM HEPES, 100 mM KCl, 1 mM $MgCl_2$, 2 mM ATP), 3.75 μL ATP regenerating mix (150 mM Creatine Phosphate, 20 mM ATP, 2 mM EGTA, 20 mM $MgCl_2$), 2.0 μL anti-photobleach (0.1 mg/mL glucose oxidase, 0.05 mg/mL catalase, 2.5 mg/mL glucose), and 3.75 μL of monomeric actin. The Giant Vesicles which have been incubated in an equal volume of ActA for 20 minutes to one hour are added to this mixture. Actin (Rabbit Skeletal Muscle, G150 Purified, Cytoskeleton, Denver) is diluted to 3.3 mg/mL in depolymerizing G-Buffer (5 mM Tris pH 8.0, 0.2 mM $CaCl_2$, 1 mM dithiotheitol (DTT), 0.2 mM ATP) for between 45 minutes and 3 hours. For experiments with fluorescent actin, actin is mixed 10:1 v/v with rhodamine actin (Cytoskeleton). The final concentration of actin is (190 ± 20) μg/mL. This concentration is much higher than the critical actin concentration (8 μg/mL) (Ref 4).

Experimental Setup

All experiments were performed at room temperature (22 ± 3 °C). The holder was designed to fit extremely snugly into the microscope stage: a 0.060" sheet of aluminum with outer dimensions 1.18" x 3.04" and inner dimensions of 0.74" x 1.45". All tolerances are to within 10 thousandths of an inch. A Press-to-Seal Silicone Isolator (Grace Biolabs, Bend, Oregon), measuring 9 mm diameter and 0.5 mm height, with adhesive was attached to a 24 mm x 60 mm No. 1 coverslip (Corning) to form a 48 μL chamber. The chamber was filled with an excess of motility assay and then with 3-4 μL vesicles coated with ActA. A 18 mm x 18 mm No. 1 coverslip covered the chamber. The coverslip was attached to the holder with vacuum grease.

The holder was gently attached to the stage (Prior Scientific, Inc, Rockland, MA) of a TE2000 inverted microscope (Nikon). The sample was initially viewed with a 20x Ph1 objective and then with a 100x Ph3 objective. The vesicles are viewed in Phase Contrast and Epifluorescence. Our chamber height is (600 ± 100) μm. This is a particularly deep chamber which allows the Giant Vesicles to localize under gravity at the chamber bottom, but does not squash even very large (100 μm) vesicles. The tall sealed chamber eliminates evaporation and permits the potential introduction of transfer pipettes into our system. Concerns with the tall system include drifting of the vesicles, temperature and chemical gradients and increased optical distortions. Nevertheless, vesicles were stationary in a sufficiently flat chamber, and gradients were prevented by a thorough mixing of the ingredients and a low light intensity on the microscope.

Our fluorescent images were taken using a mercury lamp (Nikon) and the fluorophores rhodamine, NBD and Oregon Green. The rhodamine images were taken with a TR filter cube and the NBD and Oregon Green images were taken with a GFP filter cube and sometimes a YFP filter cube.

Image Acquisition

Images were obtained and analyzed in METAMORPH (Universal Imaging, Inc.). 3D deconvolutions were performed with AutoDeblur (AutoDeblur 9.3, AutoQuant Imaging, Inc., Troy, NY). Most slices were obtained at spacings ranging from 0.29 μm to 0.44 μm per slice[4]. The resolution limit of our setup is 0.27 μm per slice. Despite greater photobleaching and taking a longer time for additional slices, there is a considerable advantage in increased resolution.

Methods of Analysis

Image Analysis

The phase contrast, rhodamine-actin fluorescence and NBD-lipid fluorescence images were compared to find and align distinctive features in each. The most accurate thickness of the actin gel was found by measuring the inner diameter (in phase contrast) and the outer diameter (in rhodamine-actin fluorescence) of the structure. For a non-spherical vesicle, the diameter was given by the average of measurements along the object's long and short axes. Lengths were measured with the measuring tool in METAMORPH. Measurement error was estimated from a combination of the pixel resolution and repeated measurements of each data point. The relative error was obtained by adding the measurement errors in quadrature.

Definition of time and uncertainty in time measurements

Time is defined as beginning at the first visible signs of a collapse (see Experimental Results). There is uncertainty in measuring the exact time of the onset of the collapse due to the present unpredictability of which structures collapse when, to the presence of many interesting simultaneously collapsing structures, and to the limited number of images taken of each structure prior to a collapse. In measurements presented here, the resolution of the time of onset varies from ±5 seconds to ±100 seconds. However, this uncertainty does not affect the slopes of the measurements because each Δt is known to within ±0.5 seconds. Additionally, since points prior to the collapse produce a plateau region for $t \leq 0$ seconds, these points were excluded from the linear plots.

Photobleaching affects lipid fluorescence more than actin fluorescence

We monitor the density of actin and lipids with the rhodamine and NBD fluorescence respectively. The bleed-through between NBD and rhodamine is observed to be negligible. By measuring the rhodamine-actin intensity at the outer edge of structures as a function of time, we find that the photobleaching of the rhodamine is negligible. However, the photobleaching of NBD is significant. Photobleaching occurs as an exponential decay, corresponding to a photobleaching rate of (2 ± 1) % per exposure.

EXPERIMENTAL RESULTS

Giant Vesicles are surrounded by a thick actin shell

Within minutes after insertion into the motility medium, a ring of actin is observed to form around the ActA coated vesicles. The ring is visible in phase contrast but is very clear in rhodamine-actin fluorescence. We infer an increasing density of actin from the intensity of the ring which increases in time. These rings, which 3D deconvolution reveals are actually fully coating shells, can develop further along one of three observed pathways. Some of these shells are static in time, some of the shells crumple, and some of the shells crush. If a vesicle is visibly deformed by a shell at an early stage of actin accumulation, it will always crush.

Crumpling is defined as the adoption of a polyhedral shape by the shell (Fig. 2f-g). The structure appears rigid and was observed to be rigid when aspirated by a micropipette. Although the crumpled structure has exchanged fluid with the medium, as visualized by a lack of phase contrast between interior regions of the structure and the exterior medium, the total volume of the crumpled structure is approximately equal to that of the original vesicle. Only limited motility is seen in fully crumpled vesicles.

Crushing is the phenomenon by which the vesicle appears to rupture under the compression by actin polymerization. The structure retains its outer diameter, but a thickening coat of actin moves radially inwards towards the vesicle center. The collapse is denoted by three main features: rapid actin movement toward the vesicle center, a radial pattern visible in phase contrast and fluorescence images, and a slower movement of actin density toward the vesicle center. The spherical symmetry of the structure is clear from the presence of a hole surrounded by a ring of rhodamine-actin fluorescence (Fig. 1). Subsequent to a collapse, there is always a heightened motility of small comet tail forming vesicles away from the crushed vesicle's center.

Crushing is a dynamic process

A representative collapse is shown in Fig. 2 for the first five minutes of crushing. Spherical vesicles tend to crush symmetrically around their center while ellipsoidal and ovoidal giant vesicles tend to crush symmetrically around two origins (Fig. 2f). The rings produce a compressive force on the vesicles, as demonstrated by deformed vesicles (Fig. 2). This deformation results in a non-spherical crushed structure (Fig. 1, 2). It is important to see that while the outer diameter of the actin shell remains approximately constant in time, the actin shell migrates inwards (Fig. 2). We will refer to the edge of the actin shell that is nearest the structure's center as the leading edge in analogy with the leading edge of a motile cell's lamellipodium.

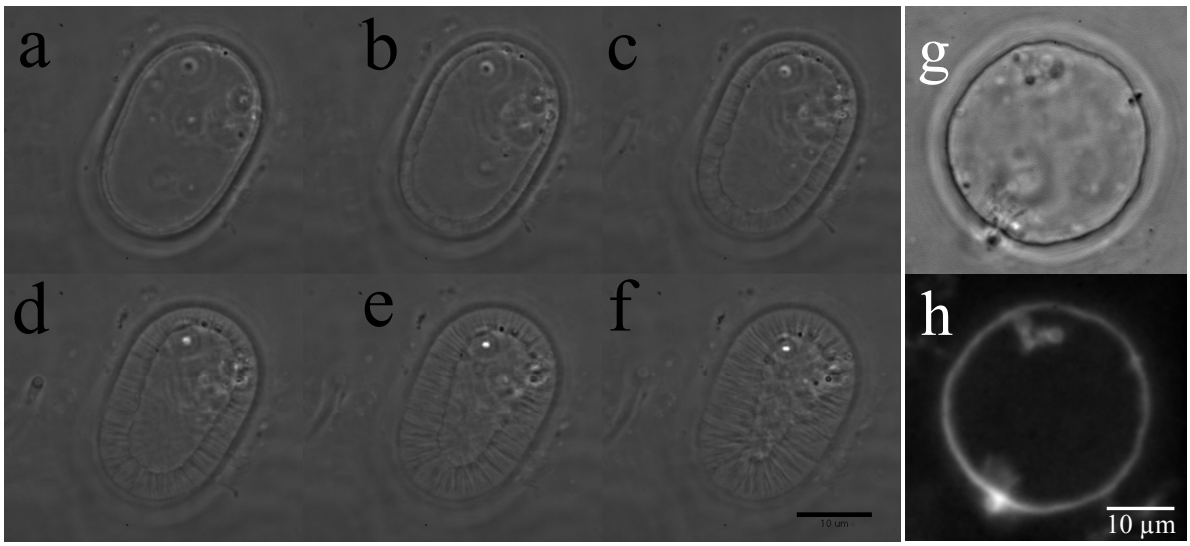

Figure 2. Time series of a collapse, and a crumpled Giant Vesicle. (a)-(f) Phase contrast images of the first five minutes (55 s per frame). The first frame is at t = (16 ± 5) s after onset of collapse. A lower bound for the velocity of the 1 µm vesicle on the left of images (c)-(f) is 1 µm/min. Scale bar is 10 µm. (g) Phase contrast image of the central plane of a crumpled vesicle several minutes after crumpling (h) Deconvolved Rhodamine-actin fluorescence

Crushing vesicle's structure observed in two-color fluorescence

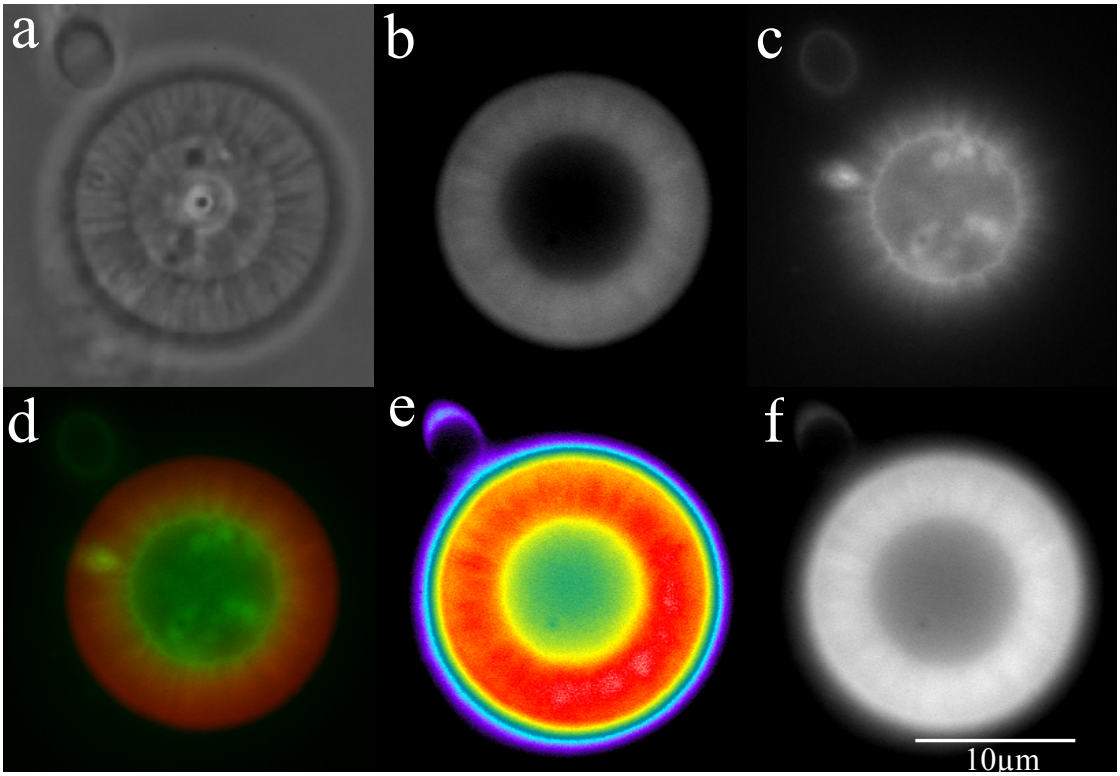

Figure 3. A GUV in mid-collapse. (a) Phase contrast (b) Highest intensities of rhodamine-actin fluorescence (c) NBD-lipid fluorescence (d) Fluorescent overlay of actin in red and lipid in green (e) Intensity profile of rhodamine-actin fluorescence (f) rhodamine actin fluorescence
Note the radial lines and the actin and lipid localization and intensity.

Figure 3 shows several simultaneous views of the same Giant Vesicle during a crushing event. Figure 3a shows a phase contrast image. The overlay of rhodamine-actin and NBD-lipid images shows the location of the actin and phospholipids during a crushing event. The position of the lipids shows that the bulk of the lipids are carried inwards towards the center of the vesicle (Fig. 3c). Many small vesicles are visible inside the lipid area. They may have been present before or they may have budded off during the crushing (Fig. 3c). Other parts of the lipid are stretched into the actin bulk as tethers. The actin density (Fig. 3e) shows a clear modulation in actin density as a function of polar angle, however the value of the periodicity appears to have a large variance. Although the outer diameter of the actin (Figs. 3a-b) is approximately constant in time, the outer diameter of the lipid structure (Figs. 3c-d) decreases with time.

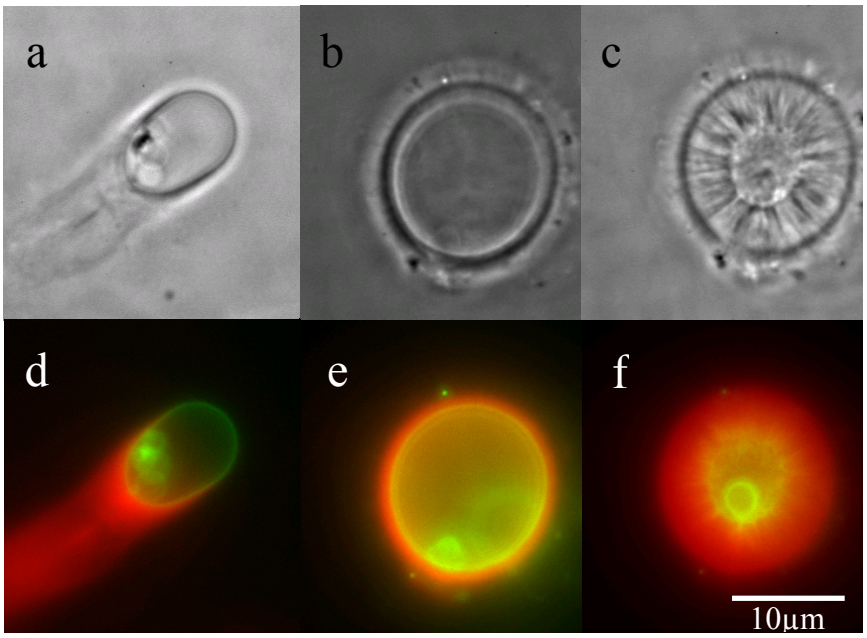

Figure 4. Comet tails and crushing in phase contrast and fluorescent overlays (a,d) Comet tail of a 10 µm Giant Vesicle (b,e) Initial stages of collapse of a 18 µm Giant Vesicle (c,f) Same vesicle partially crushed after 220 s.

Small Giant Vesicles form comet tails and large Giant Vesicles collapse

The determination of whether a Giant Vesicle will form a symmetric shell and be crushed or break symmetry and form a comet tail depends on the vesicle size. In the extreme limits, vesicles under 5 µm always form a comet tail and vesicles over 15 µm are observed always to collapse. There is an intermediate range (Fig. 4) in which Giant Vesicles are seen to exhibit either behavior. There is an exception by which very small vesicles (1-5µm) may collapse: when a large Giant Vesicle acquires a non-uniform shell, it is observed to expel a portion of its volume within a smaller vesicle. The original vesicle always collapses. If the expelled vesicle is large, it always collapses, but if the expelled vesicle is small it may form a comet tail or collapse.

The radial collapse occurs linearly in time and correlates with vesicle size

The following plots describe the transitional five to nine minutes after the onset of the collapse, and until the leading edges of the collapse overlap. The actin gel thickness increases at a constant rate (Fig. 5). The collapse velocity seems to correlate to the vesicle outer diameter. The actin gel thickness on smaller Giant Vesicles is seen to increase at a rate of 1 μm/min, whereas the actin gel thickness on larger Giant Vesicles is seen to increase at a rate of 1.5 μm/min. For comparison, velocities in the same medium for *Listeria* gives (1.9 ± 0.3) μm/min, and for comet tail forming vesicles gives (0.8 ± 0.2) μm/min (Ref 36). Vesicle geometry and external forces may affect the collapse velocity.

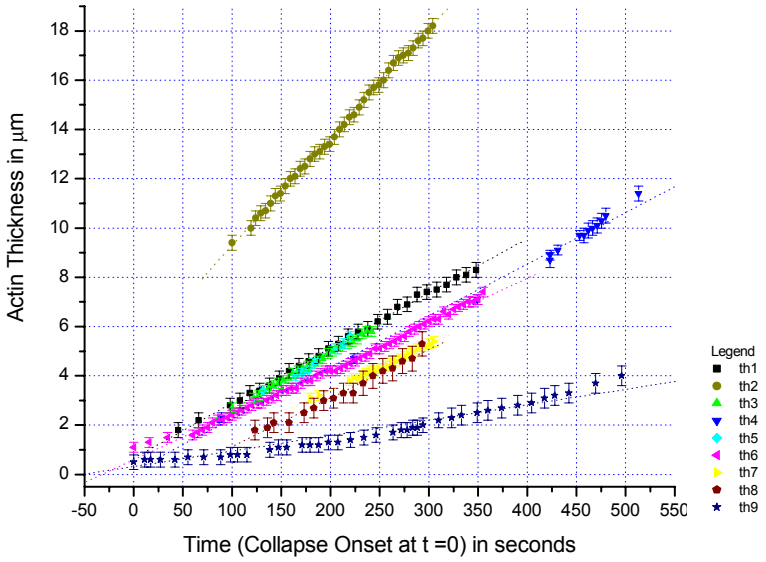

Figure 5. Plots of increase in actin gel thickness (radial velocity) vs. time.
Each color represents a distinct Giant Vesicle.

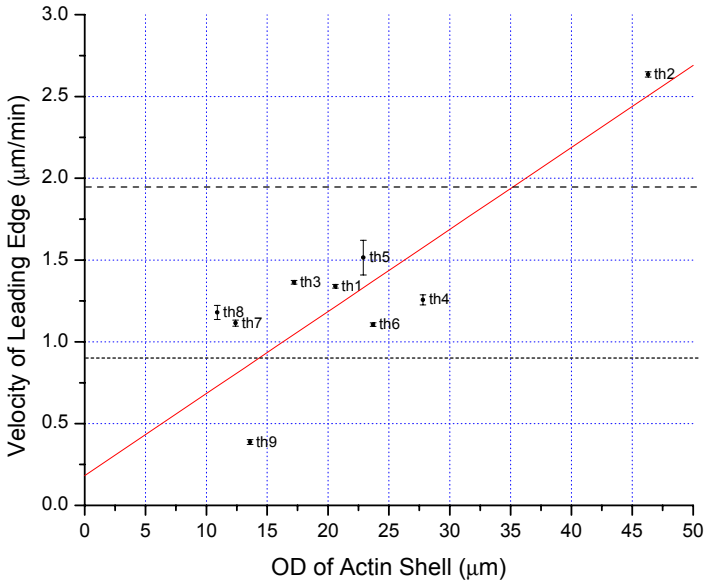

Figure 6. Collapse velocity dependence on original vesicle diameter. Larger dashed line represents velocity of *L. monocytogenes* in bovine brain extract. Smaller dashed line represents velocity of vesicles' comet tails in bovine brain extract (Upadhyaya et al. 2003). Points on Fig. 6 correspond to lines in Fig. 5.

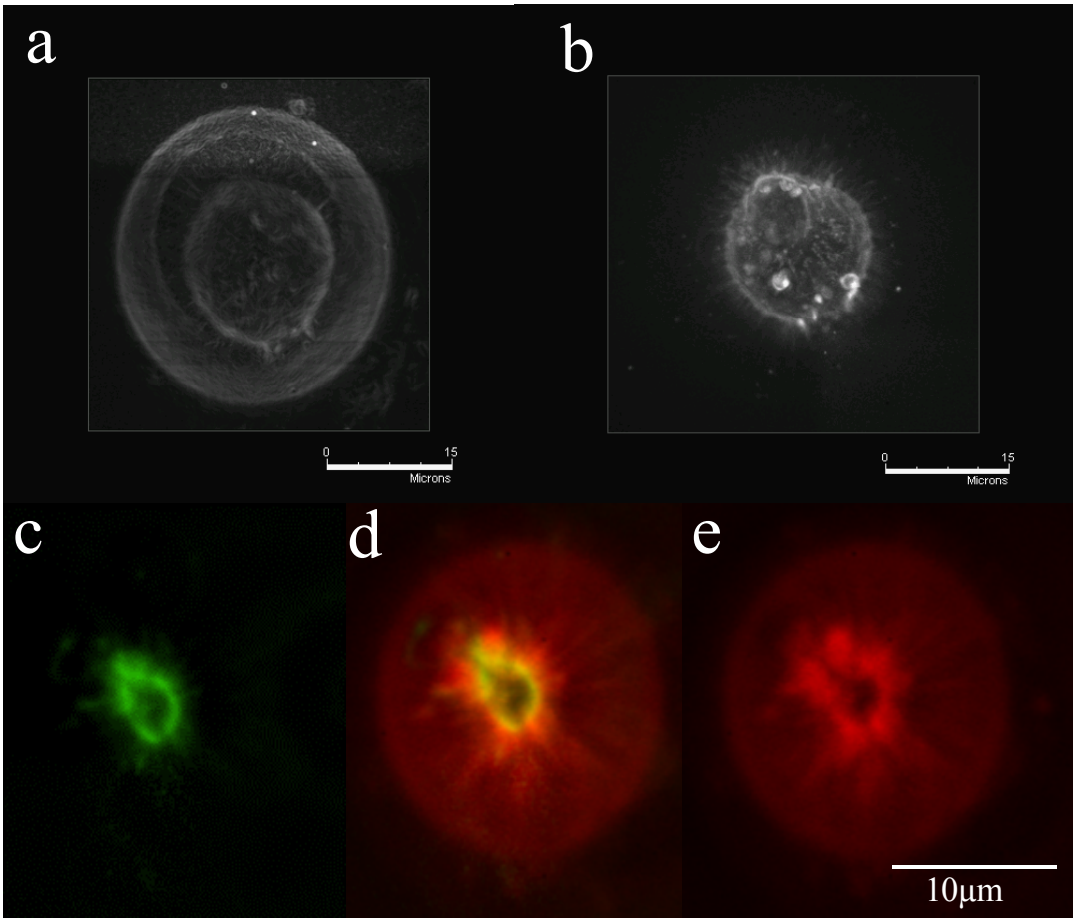

Figure 7. Actin and lipid position. Giant vesicle in mid crush as shown in 3D image of (a) rhodamine-actin and (b) NBD-lipid fluorescence. (c-e) Overlay of lipids and actin from a different small completely crushed structure. This shows the radial lines post-crush. Note the overlap of lipid fluorescence on radial actin lines.

Radial lines are observed

Radial lines are seen to be particularly intense in phase contrast microscopy, but are also visible in both fluorescent images. Measurement of these lines (Figs. 3a-c) shows a spacing of 6º per line. A careful observation of the phase, rhodamine and NBD images reveals that the highest densities of actin, lipid and phase dense contrast appear along the same radial lines. The radial lines are highly visible in a 3D image of NBD-lipid fluorescence (Fig. 7b). This is consistent with the lines being visible in several planes (not shown). The radial lines in Fig. 7 align well in Fig. 7d. It is clear that many of the radial regions of high actin density correspond to regions of radial high density of lipid. Generally speaking, the dark radial lines in phase contrast correspond to bright lines in NDB fluorescence. These bright lines in NBD also correspond well to the brightest lines in the actin fluorescence (Figs. 3a-c).

The 3D images show simultaneous actin and lipid images of a completely crushed vesicle. The colocalization of actin and lipid is especially clear in the middle overlay image (Fig. 7d).

Actin gel density spreads out and decreases in time

The properties of the actin gel and the crushed structure may be most clearly deduced from an analysis of the spatial and temporal actin density. The region of maximum intensity as a function of radius and time begins by the outer edge (Fig 8i) and decreases as it moves inwards and expands. Often, the overall actin density decreases significantly during the collapse (Fig. 8). The maximum intensity is not present at the leading edge until the collapse is almost complete. However, as the collapse reaches the milestone of closure of the central cavity, the actin density at the center of the structure increases sharply in a sustained manner (Fig. 8l).

The increase in actin density at the center of the structure does occur at the end of the collapse, whether or not the collapse is complete: Fig. 1 has maximum actin intensity at the edge of a stable central cavity. Crushed vesicles are observed to be local sources of polymerization activity for their surrounding regions, spawning many smaller comet tails.

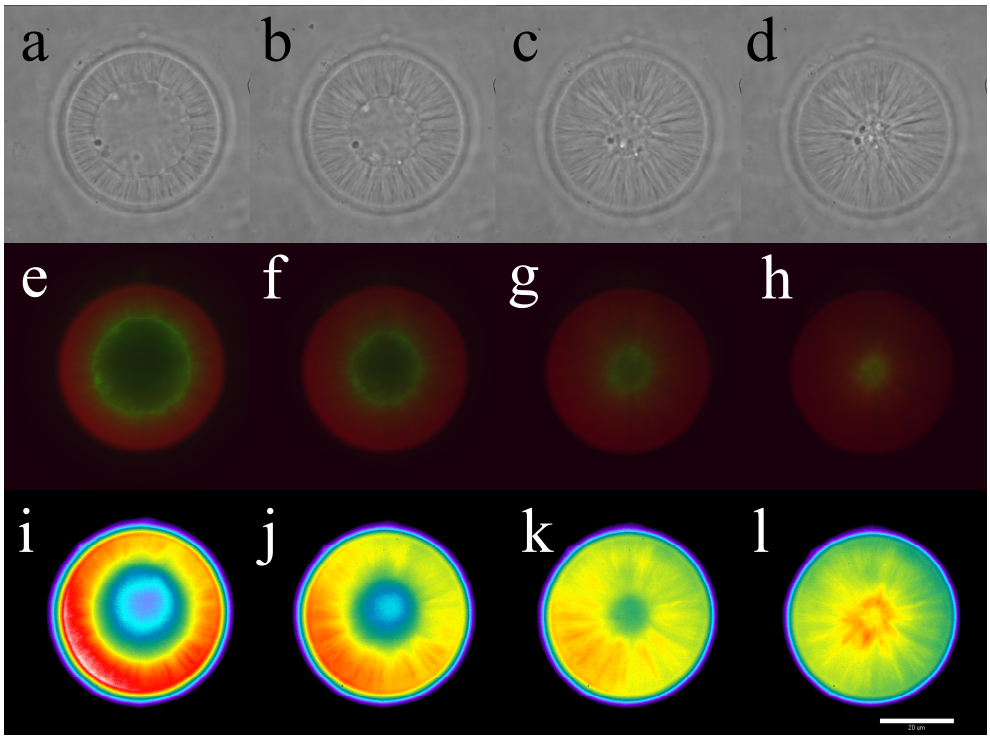

Figure 8. The collapse of a 50 um Vesicle. Phase contrast (top). Actin in red is overlayed with phospholipid in green (middle). The intensity of actin fluorescence shows the relative density of actin. Scale: 7865 (black) to 17617(white) A.U. (bottom). Pictures taken at (85 ± 1) s intervals from t = (100 ± 30) s. Scale bar is 20.

The actin density decreases at the outer radius and moves inward with slighty decreasing intensity, while the highest actin density remains in the middle of the gel (Figs. 9a-d). As the leading edge approaches the middle of the vesicle, the actin at the leading edge increases in density (Fig. 9l), becoming a major site for polymerization activity. Figures 9e-l show the actin density migrating toward the center of the structure.

Lipid and actin density

The highest density of actin is never colocalized with the highest lipid concentration during a collapse (Fig. 3b-c). However, after a collapse is complete (Fig. 7d) the maximum actin density does co-localize with the maximum lipid fluorescence. Before the collapse, the maximum density

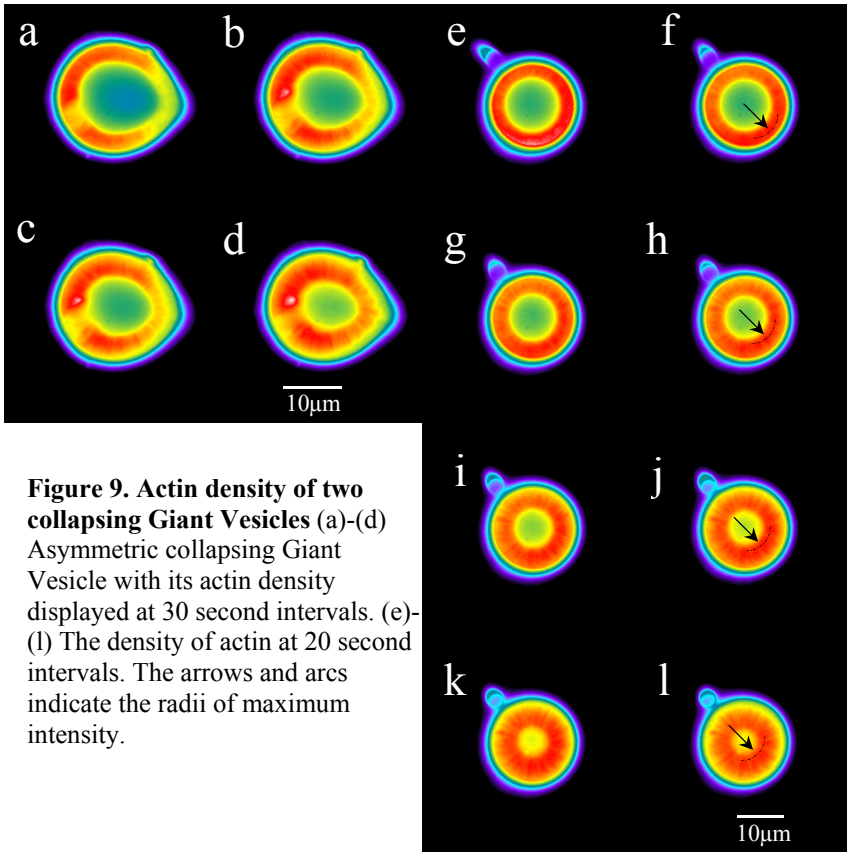

Figure 9. Actin density of two collapsing Giant Vesicles (a)-(d) Asymmetric collapsing Giant Vesicle with its actin density displayed at 30 second intervals. (e)-(l) The density of actin at 20 second intervals. The arrows and arcs indicate the radii of maximum intensity.

of actin is located just outside of the giant vesicle. During the early stages of the collapse, the maximum actin density decreases slightly and the actin spreading inwards has a very high density (actin density of Fig. 2, not shown). In the middle of the collapse, the gel keeps spreading and the intensity decreases significantly (Fig. 3). The overall actin density decreases and the maximum actin density moves toward the center of the structure. Figure 9f,h,j,l demonstrates the movement of the maximum actin density as it translocates inwards and disperses.

III. DISCUSSION

A COHERENT PICTURE OF THE CRUSHING PHENOMENA

We have observed the polymerization of actin shells on Giant Vesicles and the associated dynamics due to polymerization forces being exerted at the membrane interface resulting in a rupture of the membrane followed by a collapse.

Interpreting the collapse velocity

The collapse occurs in a radially symmetric fashion. The radial collapse velocity is constant in the regime between the onset of collapse and the closure of the central cavity. Understanding the dynamics of the collapse is aided by considering two regimes of actin polymerization. We first consider an ActA coated lipid surface of constant surface area, like a deflated ball, from which actin polymerization occurs. Unopposed, this surface would polymerize a constant volume of actin per unit time. This would produce an accelerating collapse, which does not match our observations.

A second situation involves actin polymerizing only at the inner lipid surface, visible in all of the two color images (Figs. 3d. & 8e-h). In this case, the unstressed polymerization would occur on a surface that is decreasing as $4\pi r^2$. Thus, the volume ($4\pi r^2 dr$) that is produced in time dt would be consistent with a linearly thickening gel. Thus, we find that our constant radial collapse velocity is consistent with nearly unstressed polymerization at a surface with area proportional to the square of the cavity radius. This situation matches our observations.

Opposing forces

Osmotic pressure and tension in the lipid bilayer provide the forces opposing the actin compression before rupturing takes place. Based on information that the rate of collapse is similar to the observed velocities of *Listeria* and vesicles moving under actin polymerization (Fig. 6), the question arises, where is the load? What is the force opposing the collapse? Does the giant vesicle rupture, forming a pore, and then re-seal shrinking until osmotic pressure can again oppose the stress created in the actin gel? A calculation for a GUV pore of 1 μm^2 shows water could freely replace the volume of an open GUV within a second, given that the flux through the pore (Q) depends on both the pore radius (r) , the vesicle radius (R) and rate of decrease of the vesicle radius ($\dot{R}$) (Ref 34)

$$Q = \frac{\Delta P}{3\eta R} r^3 = -4\pi R^2 \dot{R} \qquad (6)$$

This rapid rate of flow shows that if a vesicle is ruptured, it would have to be a very local and small rupture, or else it is highly unlikely that the vesicle could contain its ions to re-form and maintain an osmotic pressure. If the load is not provided by a sealed vesicle, then an effective load may be provided by the monomer diffusion.

Radial Lines show lipid stuck within the actin gel

As the bulk of the lipids are herded toward the center of the structure, some may bud off as interior vesicles, while others stretch out as tethers into the actin gel. These tethers form the radial lines. Their presence shows the lipid is binding to the actin gel (likely attaching via ActA). The forces holding the lipid in place are likely the same compression forces observed in the smaller vesicle's tethers (Ref 13, Ref 36) and in branching phenomena (Ref 37). The high actin density surrounding these lipid tubules implies that actin is polymerizing at these locations. However, the constant velocity dictates that these tethers make only a small contribution to the total actin polymerization. The reason may be that the tethers are under stress by the bulk of the actin gel, so actin polymerizes according to Eqn. 4.

The increase in actin density at the center of a collapsed structure is consistent with a relaxing actin gel with the region of highest density moving inwards until the polymerization inwards again becomes stressed by the steric hindrance of opposing actin gel. This produces the higher actin gel density as the gel becomes stressed. However, relaxation does not appear to be a significant factor since it cannot occur over such large length (microns) and time (minutes) scales as are observed.

The collapse velocity increases with vesicle size

If we consider diffusion and stress build up within the gel, we would expect that because of limited diffusion, a large vesicle, having a thicker actin shell, would inhibit monomers from reaching the leading edge. However, larger vesicles would be under less bending stress which may increase the rate of polymerization. If we consider the radial lines, the actin polymerization there might be enough to cause the larger vesicles to crush faster. Although we expect the relaxation within the gel to be at a much faster time scale than minutes, we do see a relaxation of the actin density within the gel over the course of minutes. If gel relaxation is a significant factor, it would help larger vesicles to collapse faster. More experiments have to be performed to be able to explain the correlation between vesicle size and velocity of collapse.

Why do smaller vesicles break symmetry?

Bernheim-Groswasser *et al.* (Ref 3) found that the time to symmetry-breaking depends on the bead radius. A larger bead has a larger radius of curvature and therefore builds up less bending stress within the gel which allows thicker gels. This could cause small beads to break symmetry faster than larger beads. We see that vesicles reach very different configurations based on their size. Since vesicles are deformable, larger vesicles are able to break symmetry compared to beads of the same size.

FUTURE EXPERIMENTS

In the immediate future there are three main experiments that could elucidate some of the open questions. First, the observed symmetry-breaking in small giant vesicles could be explored. A phase diagram could be constructed illustrating symmetry-breaking pathways as a function of vesicle size and the density of ActA. When looking for symmetry-breaking, it would be very helpful to use fluorescent ActA to examine its distribution before and after symmetry-breaking.

Second, Giant Vesicles can be electroformed containing fluorescent dextran. This will reveal the dynamics of the interior fluid during crushing. There may be an advantage to visualizing the moment of collapse with a high speed camera to view possible pore formation via fluorescent lipids and fluorescent dextran. This experiment has biological relevance as it is similar to a recent study on the actin coating and compression of exocytosing cortical granules in *Xenopus laevis* eggs. Actin was visualized crushing 5 μm vesicular bodies within a eukaryotic cell.(Ref 35). Similar to fluorescent dextran, studying monomer diffusion through the gel of a crushing vesicle would be interesting to study by recovery after photobleaching of fluorescent actin. the third proposed experiment involves introducing the ActA activated motility system inside Giant Vesicles. Giant Vesicles could be swelled or electroformed in G-Buffer with actin and other motility components that are stable at low ionic concentrations. Salts (especially KCl, needed at 100mM) can be added by electroporation. ActA may be added subsequently by microinjection.

CONCLUSIONS

We have introduced a novel system to measure the forces generated by actin polymerization and have explored its interesting dynamics. We found that ActA coated Giant Vesicles form thick actin shells which in turn compress the vesicles. This force due to actin polymerization and directed at the membrane interface causes the membrane to rupture. Although smaller vesicles have been observed to form comet tails, actin polymerization had not previously

been observed to rupture vesicles. We found a transition region in vesicle size between the symmetry breaking of comet tail formation and the symmetric crushing of a vesicle rupture. We have observed the subsequent collapse, which is characterized by radial lines consisting of lipids and actin, and have found that the shell thickens inward with a constant radial velocity that depends on vesicle size. We show that actin polymerization solely at the lipids on the inner surface of the gel can explain this constant velocity. These experiments can motivate theoretical models of the distribution of stresses within an actin gel polymerizing at a membrane.

Appendix

Indium Tin Oxide Slides cleaning

ITO Slides may be cleaned with many non-abrasive or acidic cleaners. The vacuum grease and lipid residues were removed with a kim wipe. The slides were soaked in warm 10% 7X® Cleaning Solution (ICN Biomedicals, Inc., Aurora, OH) and ultrasonicated (2510, Branson Ultrasonication Corp, Danbury CT) for 20 minutes. Then the slides were rinsed several times with distilled water, and then scrubbed gently with a 2% Alconox® Detergent Powder (Alconox, Inc., New York, NY) solution. The slides in the alconox solution were ultrasonicated for twenty minutes, rinsed several times in deionized water and ultrasonicated for twenty minutes in a 10% solution of ethanol. Upon transfer to 100% ethanol, the slides soaked for 10 minutes before being transferred singly to chloroform and subsequent drying under compressed air. The ITO slides were stored under vacuum in a desiccators to prevent water accumulation on the ITO face. The glass tubes used to store lipids in chloroform and the spacers used in electroformation were cleaned in this same manner, but without the final chloroform step. The same protocol, minus the chloroform, is used to clean microcentrifuge tubes and polypropylene spacers.

---

[1] $F = 6\pi\eta Rv$ on a 2μm bead moving at 1μm/min through a viscosity of 200Pa-s.
[2] See Materials and Methods
[3] The ITO slides are Unpolished Float Glass Slides with Indium Tin Oxide coated on one surface with $R_s \leq 20\Omega$ (Delta Technologies, Ltd, Stillwater, MN). Indium tin oxide is a translucent conductive coating which allows visualization of the giant vesicle formation process.
[4] Z-unit spacings were calibrated by optimizing 3D deconvolutions on spherical 10μm polystyrene beads.

References

1. Angelova M.I, and Dimitrov D.S. Liposome Electroformation. *Faraday Discussions Chemical Society,* 81:303, 345 (1986).
2. Angelova M.I., S. Soléau, Ph. Méléard, J.F. Faucon and P. Bothorel. Preparation of giant vesicles by external AC electric field. Kinetics and applications. *Progress in Colloid & Polymer Science*, 89:127-131 (1992).
3. Bernheim-Groswasser A., Wiesner S., Golsteyn R. M., Carlier M. F.& Sykes C. The dynamics of actin-based motility depend on surface parameters. *Nature* 417, 308–311(2002).
4. Bray, Dennis. Cell Movements: From Molecules to Motility. 2nd Ed. Garland Publishing, New York, p.68 (2001).
5. Cameron, Lisa A., Giardini, Paula A., Soo, Frederick S., and Theriot, Julie A. Secrets of Actin-Based Motility Revealed by a Bacterial Pathogen. *Nature Reviews Molecular Cell Biology* 1, 110-119 (2000).
6. Cameron, Lisa A., Matthew J. Footer, Alexander Van Oudenaarden, and Julie A. Theriot. Motility of ActA protein-coated microspheres driven by actin polymerization. *PNAS* 96 (1999).
7. Carlier, Marie-France, Wiesner, Sebastian, Le Clainche, Christophe, Pantaloni, Dominique. Actin-Based Motility as a self-organized system: mechanism and reconstitution in vivo. *Comptes Rendus Biologies* 326, 161-170 (2003).
8. da Silveira, Rava, Chaïeb, Sahraoui, and Mahadevan, L. Rippling Instability of a Collapsing Bubble, *Science* 287, 1468-1471 (2000).
9. Erdem Karatekin, Olivier Sandre and Françoise Brochard-Wyart. Transient Pores in vesicles. *Polymer International*, 52, 486-493 (2003).
10. Evans, E. & Rawicz, W. Entropy-driven tension and bending elasticity in condensed-fluid membranes. *Phyical Review Letters* 64, 17, 2094-2097 (1990).
11. Gerbal, Fabien, Paul Chaikin, Yitzhak Rabin and Jacques Prost, An Elastic Analysis of Listeria monocytogenes Propulsion. *Biophysical Journal* Vol 79, 20259-2275 (2000).
12. Gerbal, Fabien, Valérie Laurent, Albrecht Ott, Marie-France Carlier, Paul Chaikin, Jacques Prost. Measurement of the elasticity of the actin tail of Listeria monocytogenes. *European Biophysical Journal* Vol 29, 134-140 (2000).
13. Giardini, P.A., Fletcher, D.A., and Theriot, J.A.. Compression forces generated by actin comet tails on lipid vesicles. *PNAS* 100, 6493–6498 (2003).
14. Haeckl W., Baermann M., and Sackmann E. Shape. Changes of Self-Assembled Actin Bilayer Composite Membranes. *Physical Review Letters* 80, 1786 (1998).
15. Helfer, E., Harlepp S., Bourdieu L., Robert J., MacKintosh F.C., and Chatenay D. Buckling of Actin-Coated Membranes under Application of a Local Force. *Physical Review Letters*, Vol. 87, 8, 088103 (2001).
16. Honda, Makoto, Takiguchi, Kingo, Ishikawa, Satoshi and Hotani, Hirokazu. Morphogenesis of Liposomes Encapsulating Actin Depends on the Type of Actin-crosslinking, *Journal of Molecular Biology*, 287, 293-300 (1999).
17. Janmey PA, Hvidt S, Kas J, Lerche D, Maggs A, Sackmann E, Schliwa M, Stossel TP. The Mechanical Properties of Actin Gels, *Journal Of Biological Chemistry*, 269 (51): 32503-32513 (1994).
18. Kocks C, Gouin E, Tabouret M, Berche P, Ohayon H, Cossart P. *L. Monocytogenes*-induced actin assembly requires the actA gene product, a surface protein. *Cell*, 68(3):521-31 (1992).
19. Kuo, Scot C. The Force-Velocity Relationship for the Actin-Based Motility of *Listeria monocytogenes*. *Current Biology*, Vol. 13, 329–332, (2003).
20. Kuo, Scot C. and Mcgrath, James L. Steps and fluctuations of *Listeria monocytogenes* during actin-based motility. *Nature* 407, 1026 - 1029 (2000).
21. Lauffenberger, D.A. and Horwitz, A.F. Cell Migration: A Physically Integrated Molecular Process. *Cell*, Vol 84. 359-369 (1996).
22. Limozin, Laurent and Sackmann, Erich. Polymorphism of Cross-Linked Actin Networks in Giant Vesicles. *Physical Review Letters*, Vol 89, 16, 168103 (2002).
23. MacKintosh, F.C., Kas, J., and Janmey, P.A. Elasticity of semiflexible biopolymer networks. *Physical Review Letters,* 75, 4425–4428 (1995).
24. Marcy, Y., Prost, J., Carlier, M.F., Sykes, C. Forces generated during actin-based propulsion: A direct measurement by micromanipulation. *PNAS*, 101(16):5992-7. Epub 2004 Apr 12 (2004).
25. McGrath, James L., Eungdamrong, Narat J., Fisher, Charles I., Peng, Fay, Mahadevan, Lakshminarayanan, Mitchison, Timothy J. and Kuo, Scot C. The Force-Velocity Relationship for the Actin-Based Motility of *Listeria monocytogenes*. *Current Biology*, Vol. 13, 329–332, (2003).
26. Miyata H, Nishiyama S, Akashi KI, Kinosita K. Protrusive growth from giant liposomes driven by actin polymerization. *PNAS* 96:2048–2053 (1999).
27. Miyata, H and Hotani, H. Morphological changes in liposomes caused by the polymerization of encapsulated actin and spontaneous formation of actin bundles. *PNAS* 89, 11547 (1992).

28. Mogliner, A., and Oster G. Cell motility driven by actin polymerization. *Biophysical Journal*, 71, 3030-3045, (1996).
29. Mogliner, A., and Oster, G. Force generation by actin polymerization II: the elastic ratchet and tethered filaments. *Biophysical Journal*, 84, 1591-1605 (2003).
30. Noireaux, V., Golsteyn, R. M., Friederich, E., Prost, J., Antony, C., Louvard, D. and Sykes, C. Growing an Actin Gel on Spherical Surfaces. (2000) *Biophysical Journal*, 78, 1643–1654.
31. Pantaloni, Dominique, Le Clainche, Christophe, Carlier, Marie-France. Mechanism of Actin-Based Motility. *Science,* Vol 292, 1502-1506 (2001).
32. Plastino, J., Lelidis, I. , Prost, J., and Sykes., C. The effect of diffusion, depolymerization and nucleation promoting factors on actin gel growth. *European Biophysical Journal*, online 9 Dec (2003).
33. Samarin, Stanislav, Romero, Stéphane, Kocks, Christine, Didry, Dominique, Pantaloni, D. and Carlier, M.F. How VASP enhances actin-based motility. *Journal of Cell Biology*, 163, 131–142 (2003).
34. Sandre, Olivier, Laurent Moreaux, And Françoise Brochard-Wyart. Dynamics of transient pores in stretched vesicles. *PNAS*, Vol. 96, pp. 10591–10596 (1999).
35. Sokac A.M., Co C., Taunton J., Bement W. Cdc42-dependent actin polymerization during compensatory endocytosis in Xenopus eggs. *Nature Cell Biology,* 5 (8) 727-732 (2003).
36. Upadhyaya, A., Chabot, J.R., Andreeva, A., Samadani, A., and van Oudenaarden, A. Probing polymerization forces by using actin-propelled lipid vesicles. *PNAS*, 100, 4521–4526 (2003).
37. Upadhyaya A and van Oudenaarden A. Biomimetic systems for studying actin-based motility, *Current Biology,* 13(18):R734-744 (2003).
38. van Oudenaarden, Alexander and Theriot, Julie A. Cooperative symmetry-breaking by actin polymerization in a model for cell motility. *Nature Cell Biology,* 1, 493–499 (1999).
39. Welch MD, Rosenblatt J, Skoble J, Portnoy DA, Mitchison TJ. Interaction of human Arp2/3 complex and the *Listeria monocytogenes* ActA protein in actin filament nucleation. *Science*, Jul 3: 281(5373):105-8 (1998).
40. Wiesner, S., Helfer, E., Didry, D., Ducouret, G., Lafuma, F., Carlier, M.F., and Pantaloni, D.. A biomimetic motility assay provides insight into the mechanism of actin-based motility. *Journal of Cell Biology*, 160, 387–398 (2003).
41. Wang, Y. L. Exchange of actin subunits at the leading edge of living fibroblasts: possible role of treadmilling. *Journal of Cell Biolology* 101, 597–602 (1985).